Appraisal of surface preparation in adhesive bonding of additive manufactured substrates

Appraisal of surface preparation in adhesive bonding of additive manufactured substrates

M. Frascio[1*], C. Mandolfino[1], F. Moroni[2], M. Jilich[1], A. Lagazzo[1], M. Pizzorni[1], L. Bergonzi[2,4], C. Morano[3], M. Alfano[5], M. Avalle[1]

1-University of Genoa, Polytechnic School, via All' Opera Pia 15a, 16145 Genoa, Italy.
2-University of Parma, via Università, 12 - I 43121 Parma, Italy
3-University of Calabria, via Pietro Bucci cubo 44C, 87036 Arcavacata di Rende, Cs, Italy
4-MaCh3D Srl, Strada S. Nicoló 19, Parma, Italy
5- University of Waterloo, 200 University Avenue West, Waterloo, Ontario N2L 3G1, Canada

**Corresponding author: mattia.frascio@edu.unige.it, University of Genoa, Polytechnic School, via All' Opera Pia 15a, 16145 Genoa, Italy. Telephone +39 010 33 52241*

Abstract

This work emphasizes the critical need of surface preparation to improve the performance of adhesively bonded 3D printed Acrylonitrile Butadiene Styrene (ABS) adherends obtained using Fused Filament Fabrication (FFF). In particular, mechanical abrasion and two different plasma pre-treatments, i.e., Atmospheric Pressure Plasma (APP) and Low-Pressure Plasma (LPP), were compared through the qualitative analysis of surface wettability, using static and dynamic contact angle measurements, and the quantitative evaluation of surface roughness measured using optical profilometry. In addition, mechanical tests were carried out using the single lap joint configuration and the interaction between the treated ABS substrates and three different adhesive materials, epoxy, polyurethane and modified silane, were carefully ascertained. The results indicated that the plasma process at low pressure (LPP) enabled a substantial decrease of contact angle ($\theta<10^o$), with little modifications of surface morphology and topography with respect to the reference solvent cleaned surface ($\theta>80^o$). The improved wetting was accompanied by a relevant increase in the joint strength. The actual mechanism of fracture shifted from adhesive failure, typical of solvent cleaned and abraded surfaces, to full cohesive failure within either the substrates of the adhesive layer. Besides, a strong influence of the adhesive selected for manufacturing was reported. Indeed, using a tough bi-component epoxy adhesive in conjunction with the LPP pre-treatment led to substrate failure, representing the largest possible enhancement of joint strength. The shear strength was over 300% of that obtained with reference solvent cleaned, and 80% larger than that recorded on abraded surfaces.

Keywords

Additive manufacturing, plastics (B), surface treatment (B), Acrylonitrile Butadiene Styrene ABS.

1. Introduction

Additive manufacturing (AM) is experiencing consistent growth since processes and materials developments can obtain potentially ready-to-be-used components. While the development of modeling and optimization techniques is increasing, less attention has been paid to the issues associated with the assemblage of AM components. The build platform's dimensions limit the size of AM parts that are usually manufactured in a single build. Large objects can be broken down into smaller sub-components that are assembled after printing to circumvent the issue. Using such a modular approach facilitates the manufacturing of multi-material components and the fabrication of complex overhangs, thus preventing the appearance of support marks on exposed surfaces. Besides, the modular approach may enable improved designs whereas the direction of the applied loading can match the build direction, along which the material commonly displays the best mechanical performance. This is a relevant factor in fatigue life, as quantified experimentally on Fused Filament Fabrication (FFF) manufactured Acrylonitrile Butadiene Styrene (ABS) specimens by Frascio et al. [1]. However, using a modular approach necessarily calls forth the use of joining strategies [2–4].

Espalin et al. [3] explored the feasibility and the effectiveness of different joining methods as solvent welding, hot air welding, ultrasonic spot welding and adhesive bonding. They concluded that FFF manufactured parts have the best compatibility with bonding methods, especially using materials containing ABS. Further work on ABS FFF adherends by Kariz et al. [4] has shown that adhesive bonding represents a promising solution for joining 3D printed components. The adhesives used were a one-component polyurethane (Mitopur E45, PU 1K; Mitol d.d., Sezana, Slovenia), a two-component polyurethane (Bison Power, PU 2K; Bison International, Goes, Netherlands) and a hot melt adhesive (DORUS KS 217, HM; Henkel, Düsseldorf, Germany). The authors demonstrated that failure was mainly affected by the adhesive type, but also by the layer thickness of the deposited material in the printing process. In particular, the highest joint strength, as determined in single-lap joint tests, was obtained using the two-component polyurethane adhesive. Moreover, the analysis of fracture surfaces highlighted that decreasing the layer thickness of deposited material was beneficial for the intra layer adhesion, while higher layer thickness could increase surface roughness thereby improving adhesion. Arenas et al. [5] proposed a methodology to select the best adhesive for ABS FFF components with respect to the intended application. Performing single lap shear and butt joint tests, they found that polyurethane adhesives provided the best response, although an acrylic adhesive was also deemed a suitable choice. Moreover, authors stated that the use of cyanoacrylate, epoxy and silicone adhesives in structural applications need dedicated assembling procedures.

Several solutions are currently explored to enhance the performance of adhesively bonded joints comprising 3D printed plastic substrates. AM's ability to craft components with complex shapes provided additional scope for research, and novel ideas were proposed to pursue enhanced dissipation in the course of failure, such as tailoring the stiffness of the adhesive [6] and the substrates [7,8]. Moreover, shaping the mating surfaces to enable beneficial mechanical interlocking is another relevant point of advantage for joining difficult to bond materials, such as polyamide [9] or ABS [10] substrates. Yet, the reliability of adhesively bonded plastics ultimately depends on surface preparation. Regardless of the joint design, surface preparation is critical to establish interfacial adhesion and largely determines joint strength and overall reliability [11]. The need for proper surface pre-treatment is even more critical for non-polar plastics materials featuring low surface energy [12]. Recent works indicated that abrasion with emery paper could enhance adhesion and promoted cohesive failure in adhesively bonded 3D printed plastics [13]. However, it is also widely recognized that plasma pre-treatments can be very effective and represent a controllable and reproducible process that allows improving interfacial interactions and joint strength for materials that are difficult to bond [14–19]. An adequately designed plasma pre-treatment can increase the mechanical strength of adhesive bonded ABS joints by modifying surface morphology, wettability, and chemical composition [14]. The most significant effects determined by the interaction between a plasma and the polymer surface include ablation, crosslinking, cleaning, and activation [15]. Concerning Low-Pressure Plasma (LPP) pre-treatment and, in particular, Atmospheric Pressure Plasma (APP) pre-treatment, Ku et al. [16] performed an experimental campaign on polypropylene substrates. The APP process could increase surface roughness and decrease the contact angle as determined using drops of demineralized water. Besides, a concurrent rise in maximum shear load was reported. Abenojar et al. [17] investigated the effects of the atmospheric plasma pre-treatment parameters on polycarbonate (PC) and ABS that were chemically formulated to be processed by injection molding. They noted that contact angle values measured with a droplet of water changed after the atmospheric plasma pre-treatment as a function of the pre-treatment speed. The APP's chemical modification was studied using X-ray photoelectron spectroscopy (XPS), and the investigation stated that the response was affected by the chemical composition, especially by the additives. The polymer formulation, often tuned for the manufacturing process, can affect the treated surface's response to the plasma. Noeske et al. [18] assessed the importance of the distance between the target polymeric surface and the nozzle. Considering the results obtained on five different polymeric substrates, they concluded that the optimal value for the distance that yields the best results exists. Concerning LPP pre-treatment, the most relevant process parameters are the working gas, the power, and the exposure time.

Mandolfino et al. [19] studied the most suitable process setups to improve bonding strength for different polymers using a radio frequency low-pressure plasma (Gambetti Kenologia, Italy). It was found that the mid-range value of the parameters gives the best performance in terms of improvement of contact angle and shear strength tests. Although a significant body of literature work focused on adhesive bonding of plastics, surface preparation for 3D printed components is a topic that still deserves further attention because of printed polymers' unique properties [20]. Optimizing the surface properties and adhesion may significantly improve the mechanical performance of additive manufactured assemblies [21]. In this work, the focus is placed on the analysis of adhesive joints comprising ABS substrates manufactured using FFF. Three distinct surface preparation methods are compared, including mechanical abrasion and plasma pre-treatments, APP, and LPP. The results, with particular reference to surface roughness, wettability, assessed using static and dynamic contact angle measurements, and joint strength, were compared with the reference properties established through a standard solvent cleaning process (Loctite SF7063, Henkel, Milan). The comparative analysis also includes three different kinds of structural adhesives, which feature relatively distinct mechanical behavior.

2. Materials and methods

2.1. Materials

The FFF technology was used for manufacturing of ABS substrates. The 3D printer Wasp 4070 Industrial (Wasp, Massa Lombarda) and ABS filaments (Sienoc, Hong Kong, China) were employed throughout this study. The 3D printer is provided with a delta kinematic scheme to lay down the filament layer-by-layer and build 3D components. Moreover, it features a closed building volume and a heated building plate, which improves the reproducibility of the manufactured components.

The specimens were modelled in Creo Parametric 2.0 while the slicing was performed with Ultimaker Cura (ver. 3.5.1). Preliminary experiments were carried out according to a Taguchi L_9 orthogonal array (OA) to investigate the effect of processing variables, such as the layer height, the nozzle temperature, and the deposition speed, on the tensile strength of the 3D printed ABS. In particular, three levels for each of the above variables were considered, including their interactions. The minimum, mean and maximum of each variable were selected based on the specifications disclosed by the manufacturer. The obtained data was finally analysed by means of the Analysis of Variance (ANOVA) that yielded the processing parameters reported in **Error! Reference source not found.** [20].

Table 1: Manufacturing parameters employed in the FFF process.

Printing parameters	
Layer height (mm)	0.25
Nozzle temperature (°C)	250
Print speed (mm/s)	120

The mechanical properties of the 3D printed ABS were carefully determined through tensile tests performed following the procedure and recommendations reported in the standard UNI EN ISO 527-2:2012. An electro-mechanical testing machine Zwick Pro Line (Zwick Roell, Genoa, Italy) fitted with a 10 kN load cell was employed to perform displacement-controlled tensile tests at a cross-head displacement rate of 5 mm/min. A schematic of the dogbone samples employed in the experiments is given in Fig. 1. Five repeated tests were carried out to ensure consistency of the experimental data, and the obtained results read as follows: tensile modulus, E=(2.32 ±0.17) GPa, ultimate stress, S_{ut}=(33 ± 0.7) MPa, and strain at failure, ε_f=(5.1 ± 0.9) %, respectively. These results are consistent with the data obtained by Kariz et al. [4] performing tests on ABS FFF specimens, and very close to that obtained on injection-molded ABS samples [22].

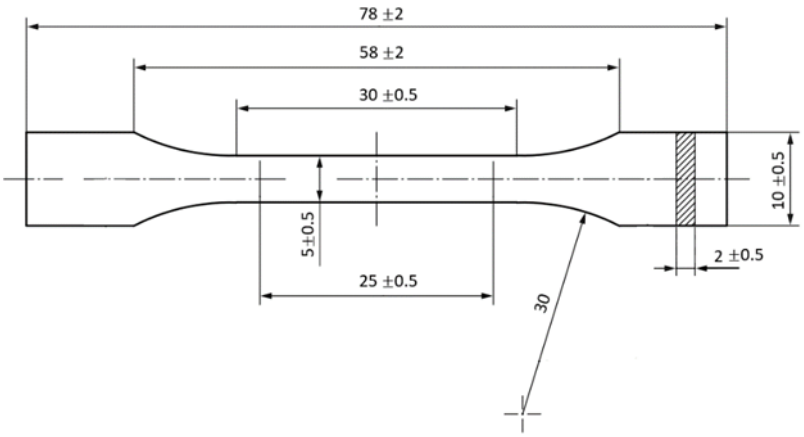

Fig. 1: Schematic of the dogbone sample manufactured according to UNI EN ISO 527-2:2012.

Adhesive bonded joints were prepared using three distinct commercial adhesives provided by Henkel Italia Srl (Milan, Italy) were considered, i.e., the Loctite EA 9466 bi-component epoxy adhesive, the Teroson 9225 polyurethane adhesive, and the Teroson MS 9399 two-component adhesive based on silane modified polymers. All these adhesives can be successfully cured at room temperature, thus avoiding exposure of the substrates to detrimental thermal effects. The viscosity of the adhesives was determined using a rotational and oscillatory rheometer Anton Paar Physica

MCR 301 (Anton Paar Italia S.r.l, Torino) equipped with a truncated cone and plate geometry (50 mm in diameter, 2° of angle, gap of 0.210 mm between the rotor and the plate). Besides, the mechanical properties of the adhesives, including the tensile modulus and the ultimate strength, were determined by performing tensile tests on dogbone samples obtained using a mold. Notice that the samples had similar dimensions of that reported earlier in Fig. 1 (UNI EN ISO 527-2:2012). Five samples for each adhesive type were tested and the results are summarized in Table 2.

Table 2: Summary of the investigated adhesives and relevant info, from the datasheet and experimental assessed, for selection.

Adhesive	**Technology**	**Fixture time (s) (ISO 4587:2003)**	**Cure time (hours) at 22 °C**	**Tensile modulus (MPa)**	**Ultimate tensile strength (MPa)**	**Viscosity (Pa*s)**	
Loctite EA 9466	Epoxy polymer	10800	24	2190.4 ± 13.7	39.2 ± 1.6	A component	28
						B component	5.8
Teroson 9225	Polyurethane polymer	1800	5	576.9 ± 16.1	13.3 ± 0.3	A component	800
						B component	60
Teroson MS 9399	Silane-modified polymer	30	24	9.3 ± 0.2	3.1 ± 0.2	A component	10
						B component	20

2.2. Surface pre-treatments

The surface pre-treatments employed in the present study are summarized in Tab. 3. The reference surface preparation is represented by a solvent cleaning process (Loctite SF7063, Henkel, Milan) whereas the substrates are wiped along the direction of the major dimension with a linen cloth. The solvent cleaning process was used to establish reference conditions for subsequent comparative analyses. Besides, mechanical abrasion using SiC emery paper, as well as APP and LPP.

Table 3: Surface pre-treatments employed.

Pre-treatment	Parameters
Cleaning	Solvent cleaning (Loctite SF7063) and wiped along the major direction
Abrasion	Solvent cleaning, then abraded with a SiC grinding paper #320 orthogonal respect to the main direction as described in ASTM D2093-03 (17), followed by further solvent cleaning
APP	Process and cooling gas: air (29 and 24 l/min respectively), power 300 W, 10 mm nozzle adherend distance, nozzle speed 50 mm/s
LPP	Solvent cleaning. Plasma parameters: working gas Air flow rate of 25 cm^3/min, power 150 W, exposure time 180 s, pressure 0.6 mbar

The abrasion pre-treatment has been performed according to the guidelines reported in the ASTM D2093-03(17). Then, two different plasma pre-treatments were carried out. In particular, APP pre-treatment (Fig. *2*a) was performed using a radio frequency low pressure plasma (Gambetti Kenologia, Italy) system with a generator power equal to 300 W. Air was used as a processing and cooling gas.

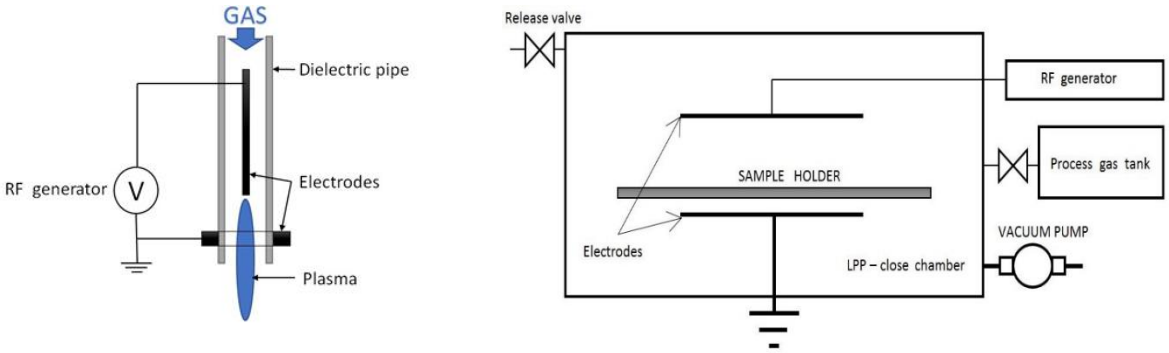

(a) (b)

Fig. 2: Plasma functional diagrams, Atmospheric Pressure Plasma (a) and Low Pressure Plasma (b).

The target surface of the samples received APP pre-treatment by moving the adherend following a grid pattern, with a spacing equal to 3 mm, using a custom-made translational x-y stage (Fig. *3*). The chosen parameters were selected by optimizing the procedure as suggested by Noeske et al. [18] and Bagiatis et al. [23], in particular using a distance of 10 mm between the nozzle and the treated surface, and line speed equal to 50 mm/s.

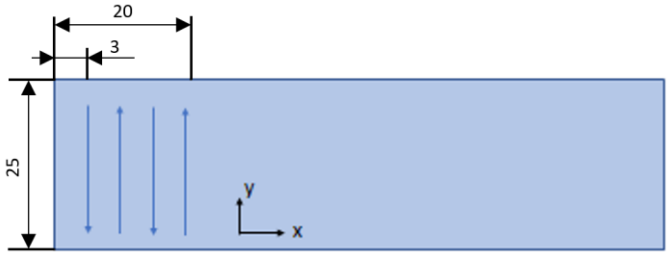

Fig. 3: Plasma jet pattern on the ABS adherend, dimensions are expressed in mm.

LPP pre-treatment (Fig. *2*b) was performed with a radio frequency RF generator (Gambetti Tucano, Italy) operating at 13.56 MHz and maximum power of 200 W. On the basis of previous experience, presented in the work of Mandolfino et al. [19], the pre-treatment was performed using a power level of 150 W and an exposure time of 300 s. Air flow rate of 0.025 SLM and a process pressure of 0.6 mbar were employed throughout the process.

2.3.Single lap shear tests

The single lap joints were designed according to the Standard ASTM D3163-01(14) and a schematic of the joint with relevant dimensions is reported in Fig. 4. Built-in alignment tabs were directly 3D printed with the ABS substrates. The adherends were subjected to the surface pre-treatments specified in Table 3 and described in the previous section. After surface the pre-treatment, the joints were assembled using jig to ensure a 0.25 mm bondline thickness. Curing and adhesive hardening was achieved following the guidelines specified in the adhesive datasheets. Mechanical tests were performed at a test speed of 1.3 mm/min and five repetitions for each sample configuration were done.

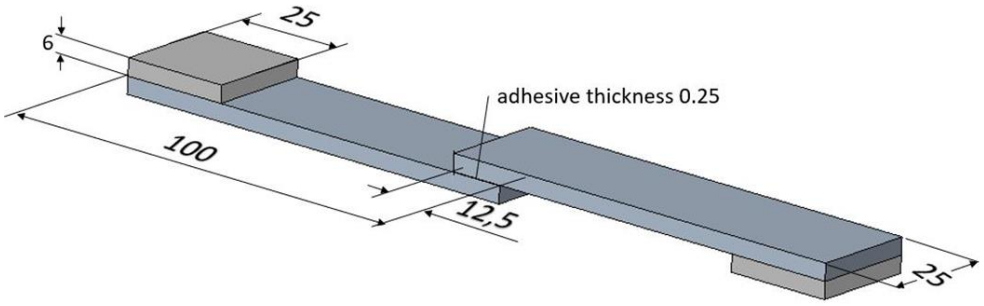

Fig. 4: Single lap shear test specimen geometry, the dimensions are expressed in mm.

The joints' average shear strength (τ_{ave}) was determined using the following equation:

$$\tau_{ave} = \frac{F_{max}}{A_0} \quad (1)$$

where A_0 was the overlap area, and F_{max} is the maximum load recorded prior to failure. For reference, monolithic single lap specimen (*i.e.*, no adhesive bonding) were 3D printed and featured the same geometry of adhesive bonded single lap joints (Fig. 4).

2.4. Surface morphology and wettability

In order to access both the morphology and topography of as produced and treated ABS, surface analysis was performed with an optical profilometer (CCI Taylor-Hobson 3D), and following the procedures reported in the EN ISO 25178 - 600:2019. The average roughness (S_a) as well as the

skewness (S_{sk}) were evaluated. These values obtained on the as-produced surfaces were used as a reference to evaluate the effect of the different surface pre-treatments.

Static and dynamic contact angles were determined to provide a characterization of surface wetting and supplement the results of mechanical tests, and the analysis of the associated mechanisms of failure Measurements were performed immediately after the surface preparation in laboratory environment at room temperature (23°C) and relative humidity (RH) 70 %. The static contact angle of metastable droplets of demineralized water placed on the target surfaces was determined from drop shape analysis. Snapshots of 2 µl calibrated water drops were taken 10 seconds after drop deposition using a microscope. For each pre-treatment, ten measurements were carried out by placing the drops at different locations across the surface, as schematically depicted in Fig. 5.

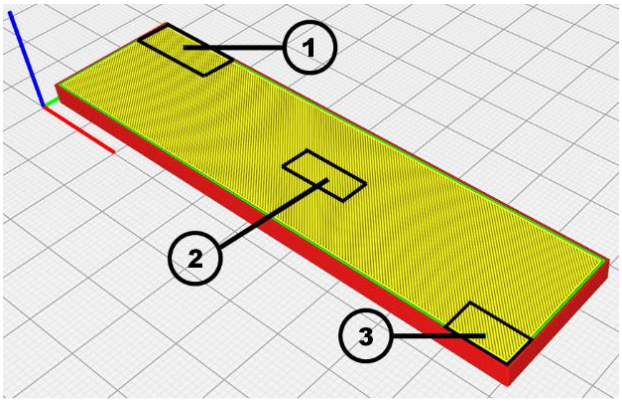

Fig. 5: Measurement positions used to obtain a relevant value of the layer surface.

The dynamic contact angle was determined based on the volume changing method and using a programmable Syringe Pump (AL-1000, Word Precision Instrument, USA). A drop of 2 µl of demineralised water placed on the surface was gradually increased in volume with a rate of 0.2 µl/s for 60 seconds, and then the volume was reduced at the same rate for other 60 seconds. Measurements were performed for all pre-treatments reported in Tab. 3, except for the LPP as for this high hydrophilic sample the deposition of a drop on its surface produces the formation of a thin film and then the evolution of the drop profile cannot be evaluated. Typical snapshots taken during the experiments are reported in Fig. 6. The advancing and the receding contact angle were determined from drop shape analysis. Three repetitions on four different samples for each surface pre-treatment were performed.

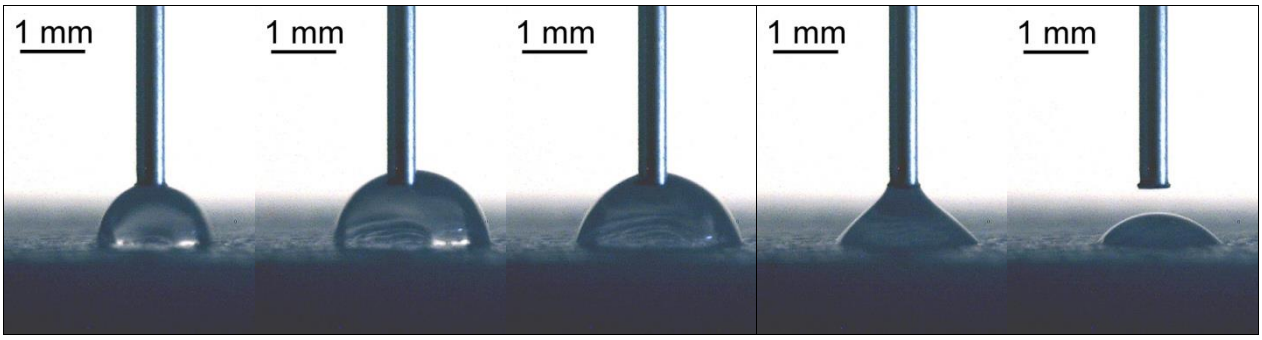

Fig. 6: Dynamic contact angle, representative sequence of the volume drop variation during the test.

3. Results and discussion

3.1. Effects of pre-treatments on surface roughness

In order to investigate the effects of different pre-treatments on surface roughness, the arithmetic mean height (S_a) was determined on the ABS surface considering the locations highlighted in Fig. 5. The mean values of repeated measurements are reported in Table 4 along with the values of skewness (S_{sk}) that represents the degree of bias of the roughness shape. Notice that the height distribution can be symmetrical around the mean plane (S_{sk}=0) as well as skewed above (S_{sk}<0) or below (S_{sk}>0) the mean plane. Comparing the data reported in Table 4 with the characteristics of the reference surface (solvent cleaned), the following conclusions can be drawn. A significant reduction of roughness occurs after mechanical abrasion because the pre-treatment leads to flattening of surface asperities. As a result, the obtained S_a is the lowest among all treated surface, and a negative value of S_{sk} also follows since the height distribution is skewed below the mean plane.

Table 4: Mean values and standard deviation of roughness after the pre-treatments.

Treatment	**Solvent Cleaned**		**Abrasion**	
	Average	Std. Dev	Average	Std. Dev
Skewness	-0.05	0.01	-1.39	0.20
S_a (µm)	11.09	1.50	5.24	1.10
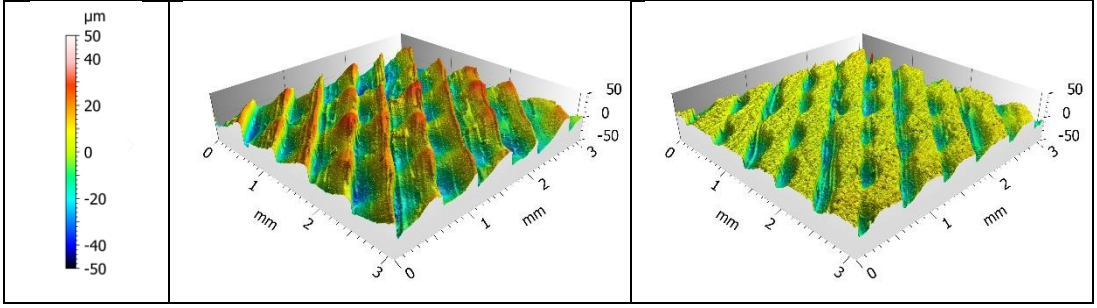				

Treatment	**APP**		**LPP**	
	Average	Std. Dev	Average	Std. Dev
Skewness	0.22	0.05	-0.56	0.15
S_a (µm)	11.06	0.79	9.51	0.33
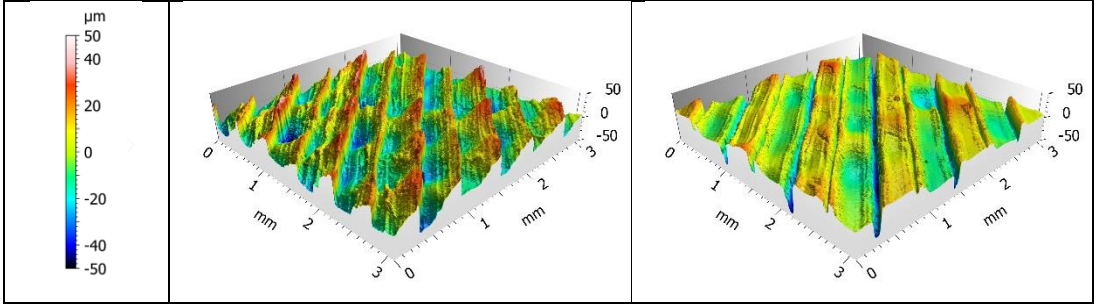				

The analysis of S_a and S_{sk} suggests that APP pre-treatment provides surface morphology almost unchanged compared to the reference solvent cleaned ABS. However, in this case the height distribution is skewed above the mean plane. The LPP pre-treatment lowers S_a and S_{sk} but compared to mechanical abrasion it seems to affect both peaks and valleys of the target surface and had a smoothing effect. Interestingly, this behaviour is in contrast with the increase of S_a observed for injection molded specimens, as reported by Mandolfino et al. [19]. The different response for the same pre-treatment can be explained considering the surface morphology before the pre-treatment. Injection molded specimens are macroscopically smooth and the LPP pre-treatment slightly increase the roughness. On the opposite, the FFF specimens are macroscopically rough and the LPP pre-treatment contributes to the flattening of the crests. It is worth noting that the peculiar FFF texture is driven by the process parameters [20] and by the deposition pattern. In particular, in this work the direction of the surface features is parallel to the fused filament deposition direction (±45° with respect to the loading direction).

3.2.Effects of pre-treatments on surface wettability

The naturally low wettability of ABS, that normally exhibits contact angles around 90°, can be substantially modified using plasma pre-treatment and, particularly the LPP, as reported in [22]. Modification of surface wettability involves both chemical and morphological aspects of a surface. For metals, the morphological aspect is more relevant [24], since the influence of the surface chemistry varies greatly from metal to metal, while for polymers, the formation of polar oxygen-containing groups, such as C-O, C=O, and O-C=O, can modify surface wettability to a large extent. Examples are reported by Mandolfino et al. [19] and Abenojar et al. [17], where XPS was performed on both untreated and APP-treated polyamide (PA) and ABS. A remarkable increase of O/C ratio after pre-treatment was recorded, which could explain the observed surface hydrophilicity.

The average values of the static contact angles and of the dynamic contact angles for each surface pre-treatment are reported in Fig. 7.

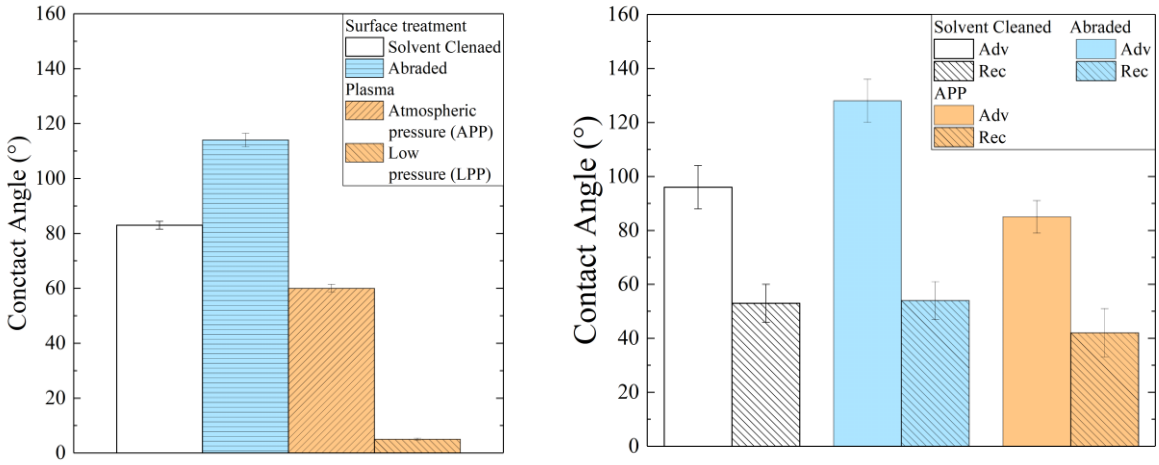

(a) (b)

Fig. 7*:* Contact angles measured after the surface pre-treatments, (a) static contact angles, (b) dynamic contact angles, advancing *Adv* and receding *Rec.*

LPP pre-treatment induces a dramatic decrease of contact angle, that prevented dynamic contact angle measurements, therefore in Fig. 7b only the measurements concerning the surface APP treated are reported. This is likely due to the chemical modification induced by plasma, as observed also on injection molded polymers [22], but also to the ability of the process to reach the valleys of the surface morphology which ensures that large portions of the target receive pre-treatment. Mechanical abrasion contributed to an apparent increase of static contact angle with respect to the solvent cleaned surface. However, considering a contact angle of the reference slightly different from 90°, an explanation of the remarkable reduction of the wettability of the surface with a change

in the roughness cannot be found in the Wenzel model [25]. Moreover, the validity of the Wenzel equation implies that the drop must be sufficiently large compared with the roughness scale, while in this case the maps of surface shows a horizontal distribution of the peaks and of the valleys of about 0.5 mm. The comparison of the receding contact angle between the two treated surfaces evidences an average value of 53° in both the samples and thus no differences can be observed. The contact angle hysteresis, namely the difference between the advancing and the receding contact angles, detects a metastability of the drop connected with the slower kinetic of the liquid penetration in the surface capillarity of the abraded sample with respect to the larger one of the reference specimens [26]. The abrasion with grinding paper #320 produces a reduction of the asperities at mesoscale level, limited to the peaks, but not changes are introduced in the valleys and an increase of the roughness are created at microscale. The higher hysteresis found in the abraded surface with respect to the one treated with the solvent is connected thus with a higher microscale roughness [26].

3.3.Shear strength, comparison of the responses of adhesives to different pre-treatments

In this section, the experimental results of the single lap shear tests are reported. The shear strength of the adhesive joint with solvent cleaned surfaces has been included as a reference to evaluate the effects of the other surface modifications. Moreover, the shear strength of the monolithic samples (no adhesive bonding), that was equal to (7.6 ±0.2) MPa, has been also included in the comparative analysis. Lap shear test results, obtained using the epoxy adhesive Loctite 9466, are reported in Fig. 8.

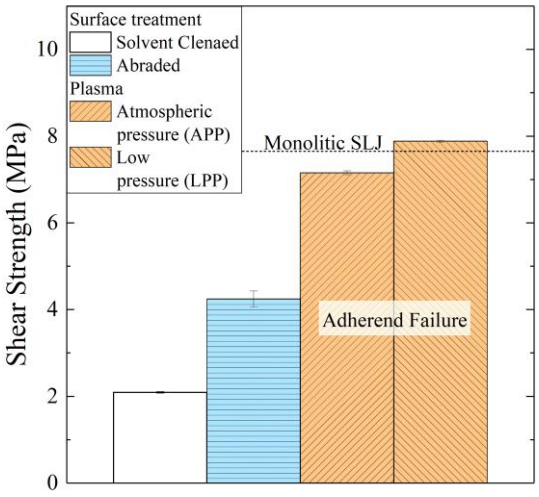

Fig. 8: Epoxy adhesive lap shear test results.

In particular, a significant increase in shear strength was achieved using both plasma pre-treatments. The mechanical strength after LPP is almost four times higher than that of solvent wiped surfaces and two times higher than that of abraded surfaces.

Mechanical abrasion reduces surface roughness, because it flattens the surface asperities at the mesoscale level and exposes the previously under surface polymeric material supposedly free of impurities and contaminations. These impurities are not necessarily removed by a simple solvent cleaning step and the establishment of weaker interfacial interactions may explain the poor performance of the reference surfaces with respect to the mechanical abraded interfaces. The increase of the water contact angle and of the hysteresis contact angle can be attributed with an increase of the coarseness of the surface abraded at macroscopic range [26].

The failure surfaces of single lap joints bonded with the bi-component epoxy adhesive are reported in Tab. 5. The survey confirmed the effectiveness of plasma pre-treatments. While solvent cleaning and abrasion with emery paper resulted in adhesive failure, plasma-treated specimens exhibited failure of the substrates, representing the maximum performance improvement.

Table 5: Epoxy 9466 failure surfaces, nominal bonding area is 25x12.5 mm.

	Pre-treatment	**Failure mode**	**Failure surfaces**
Epoxy adhesive	Cleaned	adhesive	
	Abraded	adhesive	
	APP	adherend	
	LPP	adherend	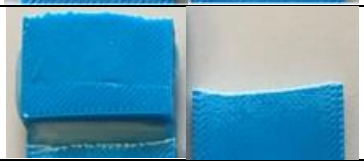

The shear strength of single lap joint bonded with the polyurethane adhesive is reported in Fig. 9. The results demonstrate that a substantial increase in shear strength can be achieved with any surface pre-treatment other than solvent cleaning. The best results were obtained with low pressure plasma pre-treatment whose corresponding average joint strength was more than three times higher than the baseline surface.

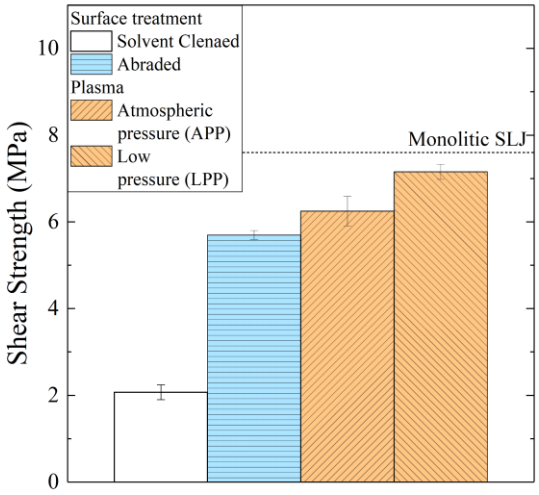

Fig. 9: Polyurethane adhesive lap shear test results.

Additional comments can be drawn from the analysis of failure surfaces reported in Tab. 6. Solvent cleaning leads to adhesive failure and low shear strength. Mechanical abrasion and atmospheric pressure plasma could provide much higher joint strength but still displayed adhesive failure. However, the failure surfaces of joints subjected to APP pre-treatment have also shown some degree of adhesive whitening, indicating the occurrence of large strains within the adhesive before failure and, thus, improved adhesion. On the other hand, LPP has led to the highest joint strength in conjunction with cohesive failure, emphasizing a higher efficiency.

Table 6: Polyurethane 9225 failure surfaces, nominal bonding area is 25x12.5 mm.

	Pre-treatment	**Failure mode**	**Failure surfaces**
Polyurethane adhesive	Cleaned	adhesive	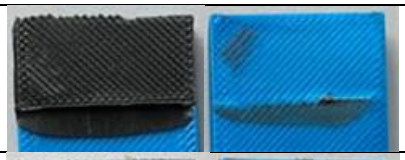
	Abraded	adhesive	
	APP	adhesive	
	LPP	cohesive	

In Fig. 10 the results of the lap shear tests for the Silane-modified Teroson 9399 adhesive joints are reported. Since it is a silane-modified adhesive, as expected, lower shear strength compared to other adhesives were recorded.

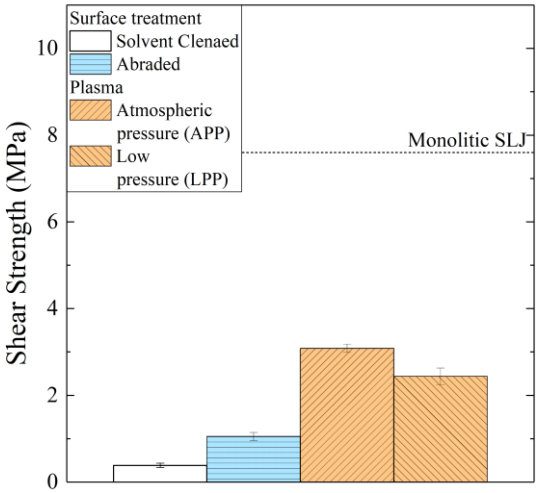

Fig. 10: Silane-modified lap shear test results.

From an analysis of the failure surfaces reported in Table 7, it is observed that solvent cleaning and abrasion are unable to promote cohesive failure, indeed, an adhesive failure was observed in all tests. On the contrary, both plasma pre-treatments led to cohesive failure of the adhesive.

Table 7: Silane-modified 9399 failure surfaces, nominal bonding area is 25x12.5 mm.

	Pre-treatment	**Failure mode**	**Failure surfaces**
Silane-modified adhesive	Cleaned	Adhesive	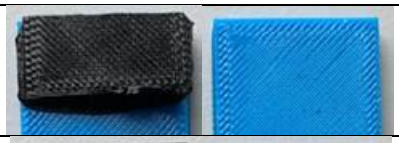
	Abraded	Adhesive	
	APP	Adhesive	
	LPP	Cohesive	

In order to summarize and compare the obtained results, the average shear stresses as a function of the surface pre-treatments examined in this work is reported in Tab. 8. The percentage variations provided in the table represent the improvements with respect to control samples. It is inferred that the shear strength of adhesive joints subjected to solvent cleaned are quite low and, as such, may be unable to ensure reliability of bonded assemblies in structural applications. This conclusion is in line with recent works by Espalin et al. [3] and Spaggiari et al. [13]. The visual inspection of failure surfaces suggests that solvent cleaning leads to purely adhesive failure. Mechanical abrasion

provided a remarkable improvement of the shear strength up to +285%. As discussed earlier, this pre-treatment decreases surface roughness removing a thin superficial layer of material that usually embeds impurities, such as additives used to improve extrusion through the nozzle, and contaminations. Although the pre-treatment may help in establishing stronger interfacial interactions, in this work the extent of the improvement was not enough to promote cohesive failure. In addition, being AM typically used to make hollow and/or lattice structures with complex geometries featuring thin walls, the risk of damage associated to subsequent mechanical abrasion could be a factor that should be accounted for while selecting a surface pre-treatment method. Moreover, in contrast to plasma technology, mechanical pre-treatments are less attractive in terms of both automation and repeatability. Regarding plasma pre-treatments, the increase of shear strength always exceed 300%. While adhesive joints subjected to plasma pre-treatment and bonded with the epoxy adhesive have always shown failure within the substrates, the polyurethane bonded joints could not achieve comparable performances. The best result was obtained with the LPP pre-treatment because it led to cohesive failure. Finally, the performances of the silane modified adhesive were mainly limited by the mechanical properties of the adhesive itself. Consistently with the other batches of samples, the plasma pre-treatments provided the best results leading to cohesive failure. The results were in good agreement with those reported in previous works [22], and further support the effectiveness of plasma pre-treatment in improving the strength of adhesive bonded 3D printed ABS.

Table 8: Results of the average shear strength τ_{av} for the different surface pre-treatment conditions and increment against control samples.

Adhesive	**Surface treatment**	**τ_{av} (MPa)**	**Standard deviation (MPa)**	**Increment (%)**
Epoxy	Cleaning	2.1	0.03	Reference
	Abrasion	4.2	0.04	200
	APP	7.2*	0.09	343
	LPP	7.9*	0.05	376
Polyurethane	Cleaning	2.0	0.34	Reference
	Abrasion	5.7	0.21	285
	APP	6.2	0.69	310
	LPP	7.2	0.35	360
Silane-modified	Cleaning	0.4	0.09	Reference
	Abrasion	1.1	0.18	275
	APP	3.1	0.19	775
	LPP	2.4	0.38	600
*failure occurred in the adherends				

4. Conclusions

In this work, the experimental characterization of SLJs with substrates manufactured using fused filament fabrication was carried out and the effects of various surface preparation methods and

adhesive materials were examined. Three surface pre-treatments were considered, i.e., mechanical abrasion with emery paper, atmospheric pressure plasma and low-pressure plasma.

Morphology analysis based on both arithmetic mean height and skewness pointed out how the three different pre-treatments had different effect on the texture created by the FFF material deposition. The APP (S_{sk} = 0.22 µm and S_a = 11.06 µm) barely modified the surface morphology from the baseline cleaned surface; mechanical abrasion flattened the surface peaks and decreased surface roughness (S_a = 5.24 µm), while the LPP smoothed both peak and valleys leading to S_a = 9.51 µm and S_{sk} = -0.56.

Wettability has been assessed qualitatively determining both the static and dynamic contact angles. The 3D printed ABS exhibited contact angles around 90° after solvent cleaning; however, it increased following to the mechanical abrasion, to which corresponded also a growth of the difference between the advancing and the receding contact angle; this increase of the dynamic contact angle hysteresis is induced by the grinding action that, while reduce the asperities of the surface at mesoscale level, however causes an increase of microscale roughness of the specimen. Finally, values lower than 10º were observed after LPP, such decrease may be associated to the formation of oxygen-containing polar groups.

The results of mechanical tests demonstrated that abrasion with emery paper could increase the joint strength with respect to baseline solvent cleaning in a range between 200 and 285% and the visual assessment of failure surfaces revealed the occurrence of mechanical interlocking, but final failure was still interfacial. Plasma pre-treatments were proven to be the most effective and could promote cohesive failure within the adhesive layer (polyurethane and silane modified bonded joints), as well as substrate failure (epoxy bonded joints). The joint strength was increased remarkably and up to +775% with respect to solvent cleaning. In addition, the obtained results have shown that, for a given surface preparation, the mechanical behaviour is affected by the adhesive material employed for joint fabrication. For instance, adhesive joints with plasma treated surfaces and bonded with epoxy resin were characterized by adherend failure, which represents the largest possible increase in joint strength. Finally, considering that LPP and APP provided similar results, any recommendation about which one should be used will need to be based on additional considerations. The size and the shape of the component to be treated will play a role in that respect. For instance, the vacuum chamber has a limited working volume, while the plasma torch at atmospheric pressure can work also on complex surfaces.

Future works could focus on the analysis of other joint configurations, such those where failure includes the propagation of a crack such that the ascertain the failure behaviour and toughness of the joints.

References

[1] Frascio M, Avalle M, Monti M. Fatigue strength of plastics components made in additive manufacturing: First experimental results. Procedia Struct Integr 2018;12:32–43. https://doi.org/10.1016/j.prostr.2018.11.109.

[2] Frascio M, Marques EA de S, Carbas RJC, da Silva LFM, Monti M, Avalle M. Review of Tailoring Methods for Joints with Additively Manufactured Adherends and Adhesives. Materials (Basel) 2020;13:3949. https://doi.org/10.3390/ma13183949.

[3] Espalin D, Arcaute K, Anchondo E, Adame A, Medina F, Winker R, et al. Analysis of bonding methods for FDM-manufactured parts. 21st Annu Int Solid Free Fabr Symp - An Addit Manuf Conf SFF 2010 2010:37–47.

[4] Kariz M, Kuzman MK, Sernek M. Adhesive bonding of 3D-printed ABS parts and wood. J Adhes Sci Technol 2017;31:1683–90. https://doi.org/10.1080/01694243.2016.1268414.

[5] Arenas JM, Alía C, Blaya F, Sanz A. Multi-criteria selection of structural adhesives to bond ABS parts obtained by rapid prototyping. Int J Adhes Adhes 2012;33:67–74. https://doi.org/10.1016/j.ijadhadh.2011.11.005.

[6] Kumar S, Wardle BL, Arif MF, Ubaid J. Stress Reduction of 3D Printed Compliance-Tailored Multilayers. Adv Eng Mater 2018;20:1–8. https://doi.org/10.1002/adem.201700883.

[7] Ubaid J, Wardle BL, Kumar S. Strength and Performance Enhancement of Multilayers by Spatial Tailoring of Adherend Compliance and Morphology via Multimaterial Jetting Additive Manufacturing. Sci Rep 2018;8:1–10. https://doi.org/10.1038/s41598-018-31819-2.

[8] Morano C, Zavattieri P, Alfano M. Tuning energy dissipation in damage tolerant bio-inspired interfaces. J Mech Phys Solids 2020;141:103965. https://doi.org/10.1016/j.jmps.2020.103965.

[9] Dugbenoo E, Arif MF, Wardle BL, Kumar S. Enhanced Bonding via Additive Manufacturing-Enabled Surface Tailoring of 3D Printed Continuous-Fiber Composites. Adv Eng Mater 2018;20:1800691. https://doi.org/10.1002/adem.201800691.

[10] Spaggiari A, Denti F. Mechanical strength of adhesively bonded joints using polymeric additive manufacturing. Proc Inst Mech Eng Part C J Mech Eng Sci 2019;0:1–9. https://doi.org/10.1177/0954406219850221.

[11] Packham DE. Surface energy , surface topography and adhesion. Int J Adhes Adhes 2003;23:437–48. https://doi.org/10.1016/S0143-7496(03)00068-X.

[12] Petrie EM. Handbook of Adhesives and Sealants. vol. 25. 1996. https://doi.org/10.1108/eb043169.

[13] Spaggiari A, Dragoni E. Effect of mechanical surface treatment on the static strength of adhesive lap joints. J Adhes 2013;89:677–96. https://doi.org/10.1080/00218464.2012.751526.

[14] Liston EM. Plasma treatment for improved bonding: A review. J Adhes 1989;30:199–218. https://doi.org/10.1080/00218468908048206.

[15] Wolf R, Sparavigna AC. Role of Plasma Surface Treatments on Wetting and Adhesion. Engineering 2010;02:397–402. https://doi.org/10.4236/eng.2010.26052.

[16] Ku JH, Jung IH, Rhee KY, Park SJ. Atmospheric pressure plasma treatment of polypropylene to improve the bonding strength of polypropylene/aluminum composites. Compos Part B Eng 2013;45:1282–7. https://doi.org/10.1016/j.compositesb.2012.06.016.

[17] Abenojar J, Torregrosa-coque R, Martinez MA, Martin-martinez JM. Surface modifications of polycarbonate (PC) and acrylonitrile butadiene styrene (ABS) copolymer by treatment with atmospheric plasma. Surf Coat Technol 2009;203:2173–80. https://doi.org/10.1016/j.surfcoat.2009.01.037.

[18] Noeske M, Degenhardt J, Strudthoff S, Lommatzsch U. Plasma jet treatment of five polymers at atmospheric pressure: Surface modifications and the relevance for adhesion. Int

J Adhes Adhes 2004;24:171–7. https://doi.org/10.1016/j.ijadhadh.2003.09.006.
[19] Mandolfino C, Lertora E, Gambaro C. Influence of cold plasma treatment parameters on the mechanical properties of polyamide homogeneous bonded joints. Surf Coatings Technol 2017;313:222–9. https://doi.org/10.1016/j.surfcoat.2017.01.071.
[20] Frascio M, Bergonzi L, Jilich M, Moroni F, Avalle M, Pirondi A, et al. Additive manufacturing process parameter influence on mechanical strength of adhesive joints, preliminary activities. Acta Polytech CTU Proc 2019;25:41–7. https://doi.org/10.14311/APP.2091.25.0041.
[21] Leicht H, Orf L, Hesselbach J, Vudugula H, Kraus E, Baudrit B, et al. Adhesive bonding of 3D-printed plastic components. J Adhes 2020;96:48–63. https://doi.org/10.1080/00218464.2019.1682561.
[22] Chlupova S, Kelar J, Slavícek P. Changing the surface properties of ABS plastic by plasma. 22nd Symp Phys Switch Arc 2017;2017-Septe:32–5. https://doi.org/10.14311/ppt.2017.1.32.
[23] Bagiatis V, Critchlow GW, Price D, Wang S. The effect of atmospheric pressure plasma treatment (APPT) on the adhesive bonding of poly(methyl methacrylate) (PMMA)-to-glass using a polydimethylsiloxane (PDMS)-based adhesive. Int J Adhes Adhes 2019;95:102405. https://doi.org/10.1016/j.ijadhadh.2019.102405.
[24] Kinloch AJ. Adhesion and Adhesives. Dordrecht: Springer Netherlands; 1987. https://doi.org/10.1007/978-94-015-7764-9.
[25] David R, Neumann AW. Contact Angle Hysteresis on Randomly Rough Surfaces: A Computational Study. Langmuir 2013;29:4551–8. https://doi.org/10.1021/la400294t.
[26] Meiron TS, Marmur A, Saguy IS. Contact angle measurement on rough surfaces. J Colloid Interface Sci 2004;274:637–44. https://doi.org/10.1016/j.jcis.2004.02.036.